CHAPTER IV
SYNTHESIS AND PHOTOCATALYTIC ACTIVITY IN METHYL ORANGE DEGADRATION OF MESOPOROUS-ASSEMBLED $SrTiO_3$ NANOCRYSTALS PREPARED BY SOL-GEL METHOD WITH THE AID OF STRUCTURE-DIRECTING SURFACTANT

Abstract

A sol-gel method with the aid of structure-directing surfactant was successfully used to synthesize mesoporous-assembled $SrTiO_3$ nanocrystal photocatalysts by using strontium nitrate ($Sr(NO_3)_2$) and tetraisopropyl orthotitanate (TIPT) as precursors. Anhydrous ethanol (EtOH), ethylene glycol (EG), or EtOH/EG was selected as a solvent, while laurylamine hydrochloride (LAHC), cetyltrimethylammonium bromide (CTAB), or cetyltrimethylammonium chloride (CTAC) was used as a structure-directing surfactant. The photodegradation of methyl orange by $SrTiO_3$ was found to be affected by the crystallinity, specific surface area, and pore characteristic. The mesoporous-assembled structure with a high pore uniformity of $SrTiO_3$ plays the most important role affecting the photocatalytic activity of the $SrTiO_3$ photocatalyst. The $SrTiO_3$ with the mesoporous-assembled structure and narrow pore size distribution synthesized at a calcination temperature of 700°C, a heating rate of 1°C min^{-1}, a LAHC-to-TIPT molar ratio of 0.25:1, and using an EtOH solvent provided the highest photocatalytic degradation activity, which was much higher than that of the non-mesoporous-structured commercial $SrTiO_3$.

4.1 Introduction

Environmental issues seem to be some of the most important topics because pollutants have been spread throughout the world, tending to accumulate in living organisms and reaching harmful levels. Technologies for the removal of environmental pollutants have been an increasingly investigated and tested means to solve these environmental problems. There are several approaches for environmental clean-up, such as adsorption, reverse osmosis, combined coagulation and

To be published in Journal of Molecular Catalysis A: Chemical, 287 (2008) 70-79

flocculation, chlorination, ozonation, electrochemical oxidation, biodegradation, and also photocatalysis [1,2]. Photocatalysis is an environmentally friendly process that utilizes radiation energy to perform catalytic reactions under ambient conditions. Thus, photocatalysis technology has been widely investigated for pollutant eradication, with emphasis on the development of effective photocatalysts [2-5].

One promising photocatalyst is strontium titanate ($SrTiO_3$) because of its superior physical and chemical properties, such as its excellent thermal stability, photocorrosion resistibility, and good structure stability as the host for metal ion doping [6]. Due to these advantages, a variety of approaches, such as the solid-state reaction technique [7], the sol-gel method [3,4,8-10], the molten salt synthesis [11], the polymerized complex technique [12], and the hydrothermal technique [13,14], have been developed to synthesize $SrTiO_3$ photocatalysts as advanced materials with specific functions to achieve good photocatalytic activity. The conventional way of synthesizing $SrTiO_3$ is based on the solid-state reaction between $SrCO_3$ and TiO_2, typically at temperatures higher than 900°C, which not only consumes high energy for its preparation but also does not permit a high degree of control and reproducibility of properties required for the photocatalysis application. This technique normally provides non-uniform particle size distribution powders and also a low degree of composition homogeneity [12,13], which affect the photocatalytic activity of the photocatalysts. In photocatalysis, there are many factors that affect the photocatalytic activity of photocatalysts, such as composition homogeneity, crystal structure, surface area, morphology (shape and size), as well as porosity and pore size distribution [2-5]. The effects of shape and size of TiO_2 on the photocatalytic degradation of methyl orange were investigated by Liao et al. [5]. Their results showed that the TiO_2 nanoparticle photocatalysts with different shapes and sizes exhibited different photocatalytic activities. For good photocatalyst synthesis, a technique based on wet chemical routes therefore seems to be more promising, especially the sol-gel method, due to the ability to control composition homogeneity, purity, shape, structure, and phase composition of the resulting powders under moderate conditions [15-17]. Several studies of the aid of surfactants in controlling the shape and size of nanocrystals have also been repoted [5,18-22]. Pileni et al. [18-21] pointed out that the use of surfactant template is an effective technique in

controlling the size, shape, and crystallinity of inorganic nanocrystals, depending on various parameters such as micelle arrangement, surfactant type, and precursor. In recent years, some researchers reported that mesoporous-structured photocatalysts can offer higher photocatalytic activity and better light-induced hydrophilicity than that of the non-porous-structured photocatalysts [8-10,22]. A new solution-based approach that has been developed to achieve mesoporous-structured materials is the sol-gel method with the aid of the structure-directing surfactant. The porosity of mesoporous-structured photocatalysts can be controlled when being synthesized by using a structure-directing surfactant via sol-gel method [8-10,23,24]. However, to our knowledge, the preparation of mesoporous $SrTiO_3$ by using this facile sol-gel method with the aid of the structure-directing surfactant, as well as its application in wastewater treatment, has not yet been reported.

This study aimed to investigate the use of a sol-gel method with the aid of the structure-directing surfactant approach for the synthesis of mesoporous-assembled $SrTiO_3$ nanocrystals with uniform particle size under mild conditions. Three types of structure-directing surfactants, namely laurylamine hydrochloride (LAHC), cetyltrimethylammonium bromide (CTAB), and cetyltrimethylammonium chloride (CTAC), were selected for this study due to their ability to assist the formation of the mesoporous-assembled structure [9,25]. Various synthesis conditions were studied with respect to the characteristics of the obtained photocatalyst. The photocatalytic activity of the synthesized $SrTiO_3$ nanocrystal photocatalysts was investigated via the photodegradation of methyl orange as a model azo-dye contaminant in a wastewater from textile industry.

4.2 Experimental

4.2.1 Materials

Strontium nitrate ($Sr(NO_3)_2$ (Wako Pure Chemical Industries, Ltd.), tetraisopropyl orthotitanate (TIPT, Tokyo Chemical Industry Co., Ltd), acetylacetone (ACA, Nacalai Tesque, Inc.), laurylamine hydrochloride (LAHC, Tokyo Chemical Industry Co., Ltd), cetyltrimethylammonium bromide (CTAB, Tokyo Chemical Industry Co., Ltd), cetyltrimethylammonium chloride (CTAC, Tokyo Chemical

Industry Co., Ltd), anhydrous ethyl alcohol (EtOH, Wako Pure Chemical Industries, Ltd.), and ethylene glycol (EG, Nacalai Tesque, Inc.) were used as starting materials. All chemicals were analytical grade and used without further purification. $Sr(NO_3)_2$ and TIPT were used as strontium and titanium precursors, respectively, for the synthesized mesoporous-assembled $SrTiO_3$ nanocrystal photocatalysts. ACA was used for slowing down the hydrolysis reaction rate of the titanium precursor. EtOH and EG were used as solvent/co-solvent media. LAHC, CTAB, and CTAC were used as structure-directing surfactants. The commercially available $SrTiO_3$ nanopowder (Wako Pure Chemical Industries, Ltd.) was also used for comparative studies on photocatalytic activity.

4.2.2 Synthesis Procedure

An equimolar ratio of ACA was first introduced into TIPT, and the mixed solution was then allowed to cool to room temperature [8-10]. A surfactant solution of LAHC, CTAC, or CTAB prepared by dissolving them in different solvents of EG, EtOH, or a mixture of EtOH and EG. Afterwards, an appropriate amount of $Sr(NO_3)_2$ was added to the surfactant solution with continuously stirring at room temperature to obtain a clear solution. The surfactant-$Sr(NO_3)_2$ solution was then slowly dropped into the yellow mixture of the TIPT-ACA solution while stirring continuously at room temperature. The resulting mixture was kept at 80°C for 2 d to obtain complete gel formation. The resulting gel was dried at 80°C for 2 d. Finally, the obtained zero gel (dried sample) was calcined at two different heating rates of 1 or 2°C min^{-1} and four different temperatures of 600, 650, 700, or 750°C for 4 h to remove the surfactant and the remaining solvent from the framework to yield the mesoporous-assembled $SrTiO_3$ nanocrystal photocatalyst (synthesized $SrTiO_3$).

4.2.3 Characterization Techniques

The thermal decomposition behavior of the zero gel and the suitable thermal treating conditions were investigated by using a TG-DTA apparatus (Shimadzu, DTG-50) with a heating rate of 10°C min^{-1} in a static air atmosphere and with α–Al_2O_3 powder used as the reference.

The crystallinity and purity of the synthesized $SrTiO_3$ and the commercial $SrTiO_3$ (Wako) were examined by X-ray diffraction (Rigaku, RINT-2100) with a rotating anode XRD generating monochromated CuK_α radiation using the continuous scanning mode at a rate of $2^oC\ min^{-1}$ and operating conditions of 40 kV and 40 mA. Crystallite size (D) was calculated from the line broadening of the corresponding X-ray diffraction peak according to the Debye-Scherrer equation:

$$D = \frac{K\lambda}{\beta\cos(\theta)}$$

where K is the Sherrer constant (0.89), λ is the wavelength of the X-ray radiation (0.15418 nm for CuK_α), β is the full width at half maximum (FWHM) of the diffraction peak measured at 2θ, and θ is the diffraction angle.

The N_2 adsorption-desorption isotherms of the synthesized $SrTiO_3$ and the commercial $SrTiO_3$ (Wako) were obtained by using a nitrogen adsorption-desorption apparatus (BEL Japan, BELSORP-18 PLUS,) at a liquid nitrogen temperature of -196^oC. The Brunauer-Emmett-Teller (BET) approach using adsorption data over the relative pressure ranging from 0.05 to 0.35 was utilized to determine the specific surface area. The Barrett-Joyner-Halenda (BJH) approach using desorption data was used to obtain a mean pore size and pore size distribution.

It is well-known that the photocatalytic activity of a photocatalyst is related to its band gap energy (E_g). Thus, the diffuse reflectance spectra of the synthesized $SrTiO_3$ and the commercial $SrTiO_3$ (Wako) were obtained by using a UV-Visible spectrophotometer (Shimadzu, UV-2450) at room temperature with $BaSO_4$ as the reference. Afterwards, the diffuse reflectance spectra were analyzed to estimate the band gap energy (E_g, eV) by using the Kubelka-Munk function ($F(R)$), as expressed by the following equation:

$$F(R) = \frac{(1-R)^2}{2R}$$

where R is the ratio of the reflected light intensity to the reflected light intensity of the reference. The band gap wavelength (λ_g, nm) was the crossing point between the line extrapolated from the onset of the rising part and x-axis of the plot of $F(R)$ as a

function of wavelength (λ, nm). The E_g was then determined by using the following equation [10]:

$$E_g = \frac{1240}{\lambda_g}$$

The synthesized $SrTiO_3$ and the commercial $SrTiO_3$ (Wako) morphologies were observed by a transmission electron microscope (TEM) (JEOL, JEM-200CX) at 200 kV. The specimens for TEM analysis were prepared by ultrasonically dispersing pestled powders of the photocatalysts in 2-propanol and then placing drops of the suspension on a Cu microgrid with carbon film.

4.2.4 Photocatalytic Activity Testing

The photocatalytic activity of the synthesized $SrTiO_3$ and the commercial $SrTiO_3$ (Wako) were investigated using the photodegradation of methyl orange in aqueous solution under UV irradiation (Vilber Lourmat, VL 115L, 15 W, with a maximum emission wavelength of 365 nm) at room temperature. A quantity of 0.15 mg of methyl orange was dissolved in 15 ml of distilled water to yield a methyl orange concentration of 10 mg l^{-1}. An amount of 0.075 mg of the $SrTiO_3$ powders was suspended in the methyl orange solution by using a magnetic stirrer, and the suspension was photoirradiated at room temperature. The sample was periodically withdrawn (sampling time of 30 min), centrifuged to separate the photocatalyst powder from the solution, and used for the absorbance measurement. The absorbance of the solution samples was monitored by the UV-Visible spectrophotometer and was used to determine the percentage of methyl orange degradation. Moreover, the pseudo-first order rate constant (k, min^{-1}) for the photodegradation reaction of methyl orange was determined through the following relation:

$$\ln\left(\frac{C_0}{C}\right) = kt$$

The k value was calculated from the plot between $\ln(C_0/C)$ and time (t), where C_0 and C denote the methyl orange concentration at $t = 0$ and $t = t$, respectively. The percentage of methyl orange degradation and the pseudo-first order rate constant

were used as the indicators for evaluating the photocatalytic activity of the synthesized $SrTiO_3$, as compared to the commercial $SrTiO_3$ (Wako).

4.3 Results and Discussion

4.3.1 Effects of Synthesis Conditions

In this work, mesoporous-assembled $SrTiO_3$ nanocrystal photocatalysts were synthesized via the sol-gel method with the aid of structure-directing surfactant in a system of surfactant-$Sr(NO_3)_2$ solution/TIPT modified with ACA using different solvents and surfactants. When TIPT is first mixed with ACA, the ACA combines with the Ti atom and leaves one isopropoxyl group. The change in coordination number of Ti atom from 4 to 5 can be determined from a color change from colorless to yellow [9,26]. The selected surfactant (LAHC, CTAB, or CTAC) and $Sr(NO_3)_2$ were dissolved in the selected solvent (EtOH, EG, or EtOH/EG) to prepare a surfactant-$Sr(NO_3)_2$ solution. For this step, a surfactant has to be completely dissolved in a selected solvent. $Sr(NO_3)_2$ was found to be completely dissolved in EG, but not in EtOH. When EG was used as a solvent, the gel did not appear but it was found to form very slowly by adding a proper amount of water. For the case of EtOH as a solvent, a certain amount of water was required to completely dissolve $Sr(NO_3)_2$, and the gel formation rate was very fast. In the case of the mixed solvents of EtOH and EG, water was not required to enhance both $Sr(NO_3)_2$ dissolution and the rate of the gel formation. The experimental results showed that the increase in EtOH-to-EG volumetric ratio (from 0.001:1, 0.1:1, 0.4:1, 0.6:1, 0.8:1, to 1:1) led to the decrease in the gelling time, indicating that the presence of EtOH can also accelerate the condensation step of the modified metal precursors to form gel. Nevertheless, if EtOH in the EtOH/EG mixture was too high (an EtOH-to-EG volumetric ratio higher than 0.6:1), $Sr(NO_3)_2$ could not be dissolved. The results suggest that EtOH seems to be the most suitable solvent to achieve the shortest gelling time and the mild synthesis conditions. However, a small amount of water is needed to enhance the $Sr(NO_3)_2$ dissolution.

The effects of heating rate and temperature for the calcination step to remove the surfactant and solvent to obtain the synthesized $SrTiO_3$ were also

investigated. The zero gels were calcined at two different heating rates of 1 and 2°C min^{-1}. The lower the heating rate for calcination, the slower the surfactant removal, resulting in the reduction of sintering and pore collapse, which leads to having a higher specific surface area about 1.5-2 times than that with the higher heating rate. As also expected, the low calcination temperature was found to give a resultant powder with a higher specific surface area than the high calcination temperature. Hence, the heating rate of $1^{o}C\ min^{-1}$ was selected for further investigation. It is hypothesized that the higher the specific surface area, the higher the photocatalytic activity.

4.3.2 Characterization Results

TG-DTA analyses of the zero gels synthesized with different solvents were carried out to study the thermal behavior, including the decomposition temperature of the organic matters and the corresponding weight loss. The TG-DTA curves of all zero gels prepared with different solvents exhibit quite a similar thermal behavior, as shown in Figure 4.1 From the DTA profiles, each zero gel sample clearly showed two main exothermic peaks and one small endothermic peak. The positions of the peaks and the corresponding weight losses of all samples are summarized in Table 4.1. The first exothermic peak of each zero gel sample is mainly attributed to the burnout of the surfactant, as well as the residue solvent. The DTA profile of the zero gel synthesized by using EG (Figure 4.1(a)) showed broad peaks, while those of the zero gels synthesized by using EtOH and the EtOH/EG mixture showed sharp and narrow peaks (Figures 4.1(b) and (c)). The difference in DTA profiles could plausibly depend on the difference in the molecular structures between EG and EtOH. Because an EG molecule contains two OH groups while an EtOH molecule has only one, the system with EG tends to have more oriented patterns in forming bonds with surrounding surfactant molecules than that with EtOH or the EtOH/EG mixture. Therefore, the system with EG requires various energy levels to remove the surfactant molecules from the zero gel. This possibly caused the peak of the gel synthesized using EG to be broader than those synthesized by using EtOH and the EtOH/EG mixture.

(a)

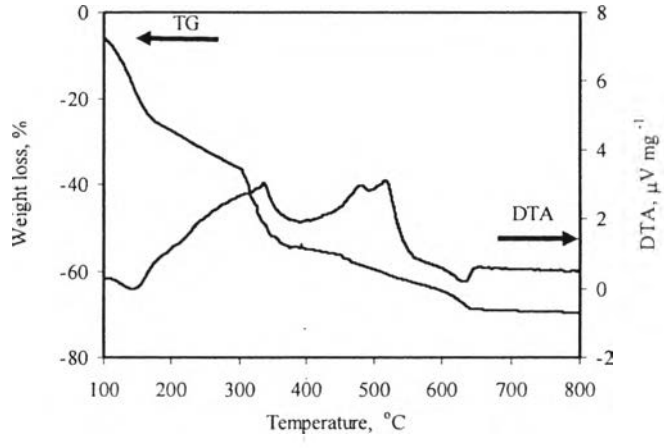

(b)

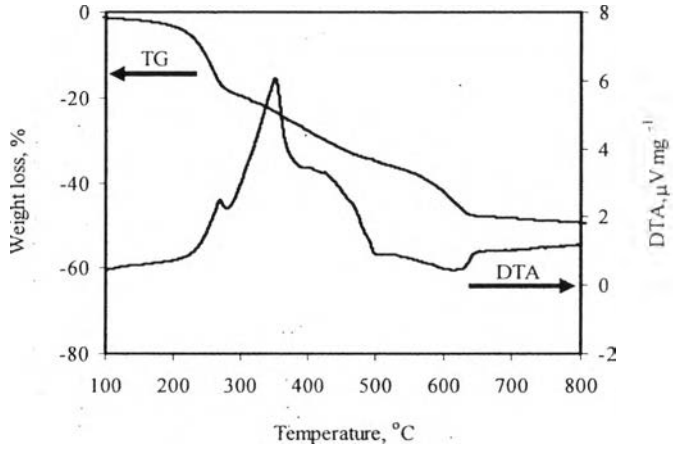

(c)

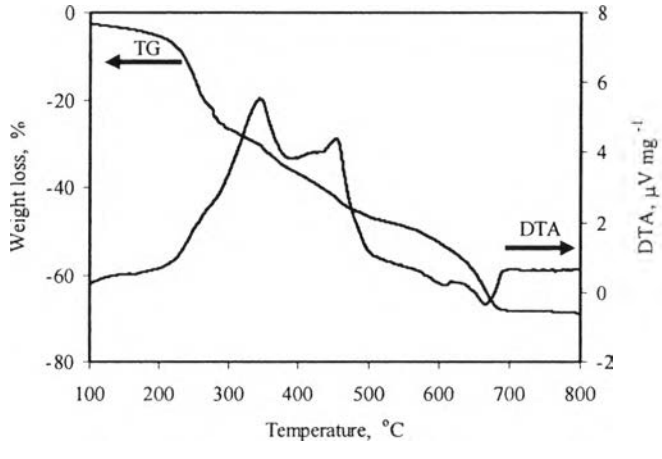

Figure 4.1 TG-DTA curves of the synthesized $SrTiO_3$ samples (zero gels) (LAHC as a structure-directing surfactant and a LAHC-to-TIPT molar ratio of 0.25:1) prepared by using different solvents: (a) EG, (b) EtOH, and (c) an EtOH/EG mixture (EtOH-to-EG volumetric ratio of 0.1:1).

Table 4.1 Thermal decomposition behaviors obtained from the TG-DTA analysis of photocatalysts prepared by using different solvents

Type of solvent used for $SrTiO_3$ synthesis	Exothermic peak				Endothermic peak		Total weight loss up to 800 °C (wt.%)
	Position (°C)		Weight loss (wt.%)		Position (°C)	Weight loss (wt.%)	
	1st peak	2nd peak	1st peak	2nd peak	3rd peak	3rd peak	
EG	336	515	49	11	634	8	70
EtOH	351	402	23	5	612	16	49
EtOH/EG	343	453	30	12	667	22	68

For each sample, the second exothermic peak is caused by the transition state due to the crystallization process of the $SrTiO_3$, as well as the decomposition of the remaining solvent that is tightly bonded in the molecular level with both Sr and Ti metals in the gel network. Since EtOH contains only one OH group, it forms a weaker bond with the metals than EG (having two OH groups). Therefore, the temperature required to remove the bonded EtOH molecules is lower, as compared to EG, and its second peak appeared to overlap with the first peak, as shown in Table 4.1 and Figure 4.1. The small endothermic peak of each sample appeared at a higher temperature than their exothermic peaks. These endothermic peaks of the samples can be ascribed to the removal of chemisorbed water molecules possibly released from the crystallization transition and/or the decomposition of the carbonate residues. The weight loss of either zero gel synthesized by using EG or EtOH proceeded up to a temperature of about 650°C, and the total weight losses of both zero gels were 70% and 49%, for EG and EtOH, respectively. These results indicate that the heat treatment at 650°C is sufficient for the formation of a well-crystallized $SrTiO_3$. For the zero gel synthesized by using the EtOH/EG mixture, the weight loss proceeded up to a temperature of about 690°C, and the total weight loss was 68.0%.

The XRD patterns of the synthesized $SrTiO_3$ using different solvents, surfactants, and calcination temperatures as compared to the commercial $SrTiO_3$ (Wako) are shown in Figures 4.2-4.4, respectively. The dominant peaks at 2θ of

about 32.4, 39.9, 46.4, 57.8, 67.8, and 77.2°, which represented the indices of (110), (111), (200), (211), (220), and (310) planes, respectively, could be indexed to the $SrTiO_3$ with a cubic perovskite structure (JCPDS card No. 35-0734) [27].

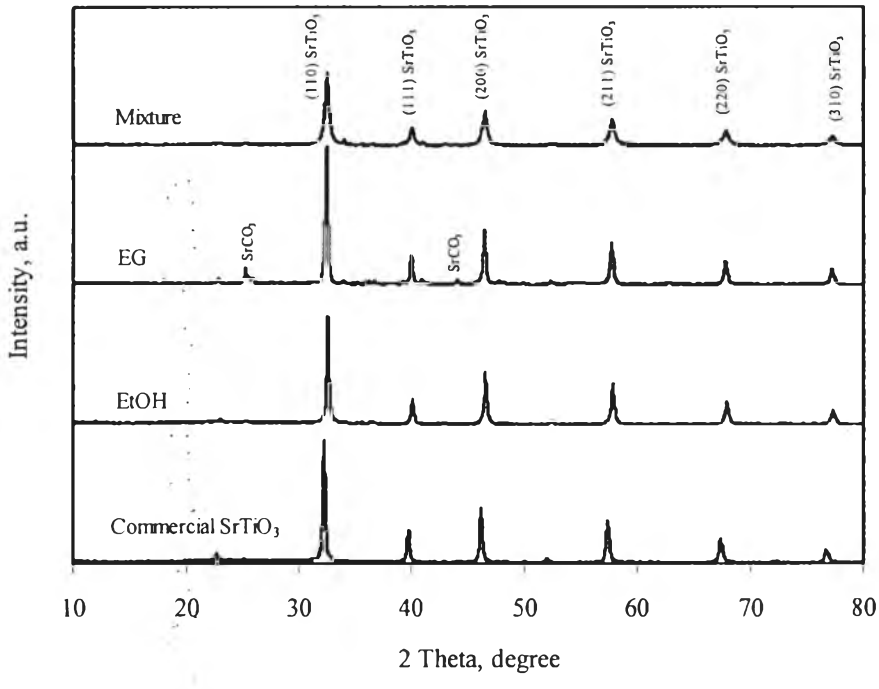

Figure 4.2 XRD patterns of the synthesized $SrTiO_3$ (a calcination temperature of 700°C, a heating rate of 1°C min^{-1}, and a TIPT-to-LAHC molar ratio of 1:0.25) prepared with different solvents: EtOH, EG, and an EtOH/EG mixture (EtOH-to-EG volumetric ratio of 0.1:1), as compared to the commercial $SrTiO_3$ (Wako).

The effect of solvent on the purity and the crystallinity of the $SrTiO_3$ synthesized at a calcination temperature of 700°C, a heating rate of 1°C min^{-1}, and a LAHC-to-TIPT molar ratio of 0.25:1 is shown in Figure 4.2. The $SrTiO_3$ synthesized by using EG was shown to contain a small quantity of $SrCO_3$ impurity. It is known that $SrCO_3$ is a common product during the preparation of nanopowder of alkaline titanates, such as $SrTiO_3$, as the $SrCO_3$ peaks at 2θ of about 25.2, 25.9, and 44.2° (JCPDS card No. 05-0418) [27] occurred in its XRD diffractogram. Interestingly, the use of the EtOH/EG mixture in the synthesis of $SrTiO_3$ provided very low $SrCO_3$ impurity. Among all investigated solvents, EtOH could produce the synthesized

$SrTiO_3$ having the highest purity but slightly lower crystallinity than that prepared by using EG. The effect of surfactant on the purity and the crystallinity of the $SrTiO_3$ synthesized at a calcination temperature of 700°C, a heating rate of 1°C min^{-1}, EtOH as a solvent, and a surfactant-to-TIPT molar ratio of 0.25:1 is shown in Figure 4.3.

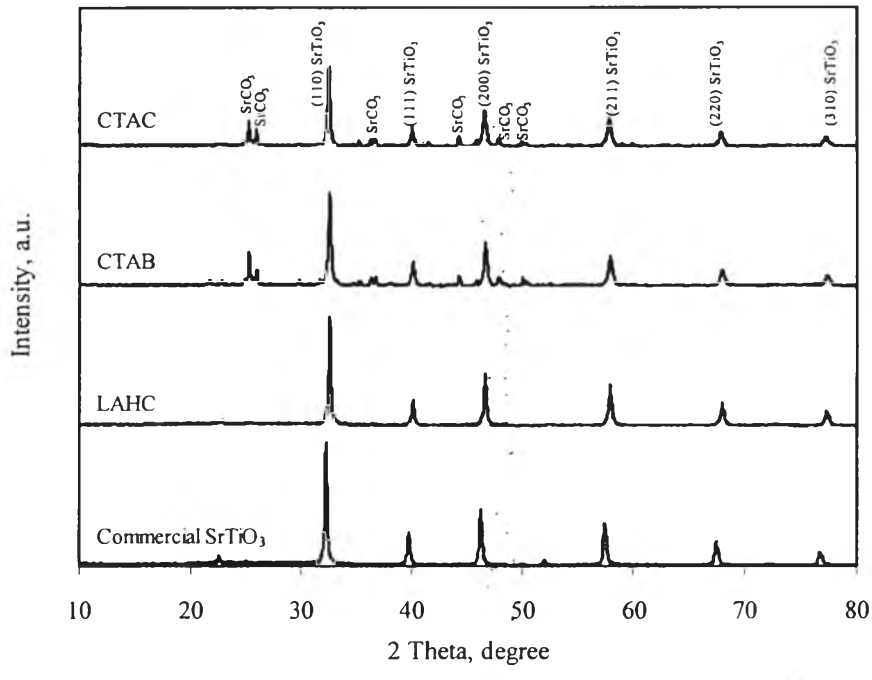

Figure 4.3 XRD patterns of the synthesized $SrTiO_3$ (EtOH as a solvent, a calcination temperature of 700°C, a heating rate of 1°C min^{-1}, and a surfactant-to-TIPT molar ratio of 0.25:1) using different surfactants: LAHC, CTAB, and CTAC, as compared to the commercial $SrTiO_3$ (Wako).

The synthesized $SrTiO_3$ using LAHC as a structure-directing surfactant showed both a significantly higher purity and crystallinity than those prepared by using CTAB or CTAC, as indicated by the XRD diffractograms. Moreover, the synthesized $SrTiO_3$ using LAHC showed no $SrCO_3$ peaks, unlike the XRD diffractograms of those prepared by using CTAB or CTAC (showing the $SrCO_3$ peaks at 2θ of about 25.2, 25.9, 36.6, 44.2, 47.8, and 50.0°). Since CTAB and CTAC are higher molecular weight surfactants with more number of C atoms than

LAHC, as well as, three branches of methyl groups in their heads, they might be more difficult to be removed from the gel network, and some C atoms might be left

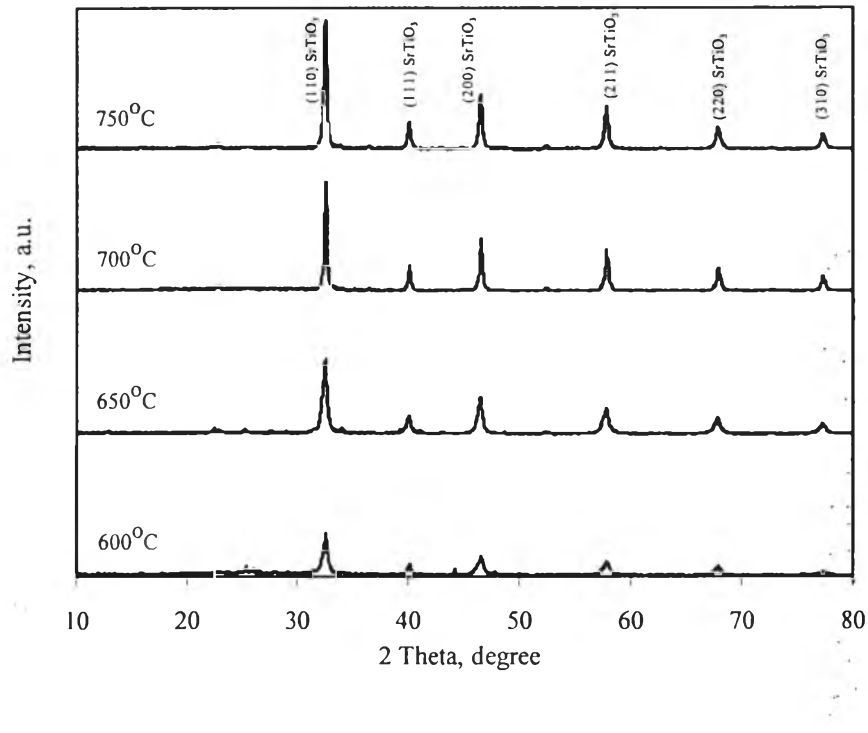

Figure 4.4 XRD patterns of the synthesized $SrTiO_3$ (EtOH as a solvent, a heating rate of 1°C min^{-1}, and a LAHC-to-TIPT molar ratio of 0.25:1) calcined at different calcination temperatures.

to react with Sr atoms to form $SrCO_3$ during the calcination step. From Figures 4.2 and 4.3, the $SrTiO_3$ synthesized by using EtOH as a solvent and LAHC as a structure-directing surfactant shows no $SrCO_3$ and other impurity peaks, indicating that both chemical structures of solvent and surfactant play important roles affecting the purity and crystallinity of $SrTiO_3$, and the use of EtOH and LAHC can offer a pure crystalline $SrTiO_3$. As shown in Figure 4.3, the $SrTiO_3$ synthesized by using LAHC shows similar XRD patterns to the commercial $SrTiO_3$. Figure 4.4 shows the effect of calcination temperature on the purity and crystallinity of the synthesized $SrTiO_3$ at a heating rate of 1°C min^{-1} and a LAHC-to-TIPT molar ratio of 0.25:1 using EtOH as a solvent. An increase in calcination temperature was found to increase both the purity and crystallinity of the synthesized $SrTiO_3$ in the studied

range of 600-750°C. In spite of the lower crystallinity (not well-crystallized) of the synthesized $SrTiO_3$ calcined at 600 and 650°C, it is surprisingly noted that the use of EtOH as a solvent and LAHC as a structure-directing surfactant could result in no impurity of $SrCO_3$, even though a low calcination temperature of 600°C was used.

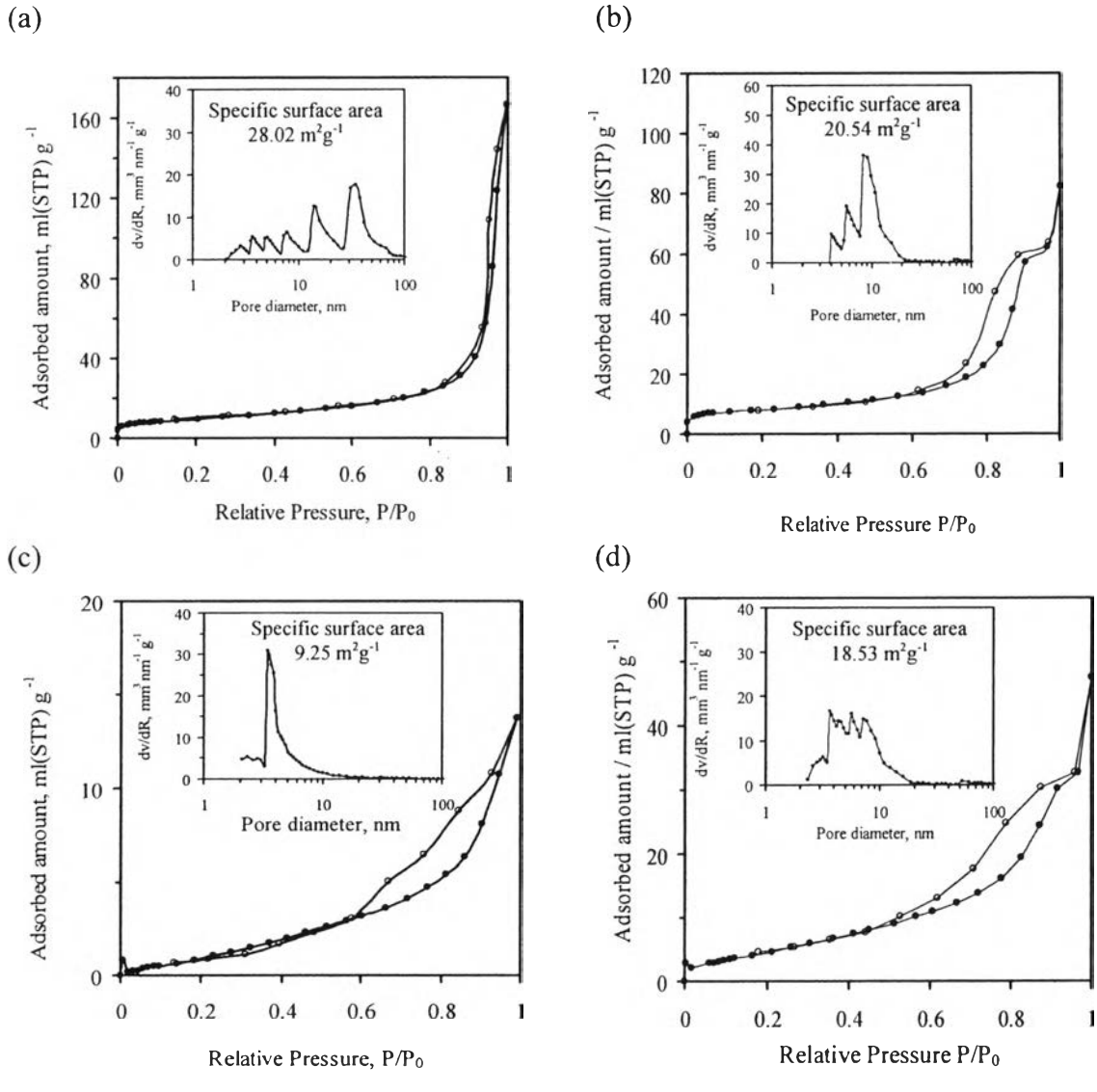

Figure 4.5 N_2 adsorption-desorption isotherms, specific surface area, and pore size distributions of (a) the commercial $SrTiO_3$ (Wako), and the synthesized $SrTiO_3$ (a calcination temperature of 700°C, a heating rate of 1°C min^{-1}, and a LAHC-to-TIPT molar ratio of 0.25:1) using different solvents: (b) EG, (c) EtOH, and (d) an EtOH/EG mixture.

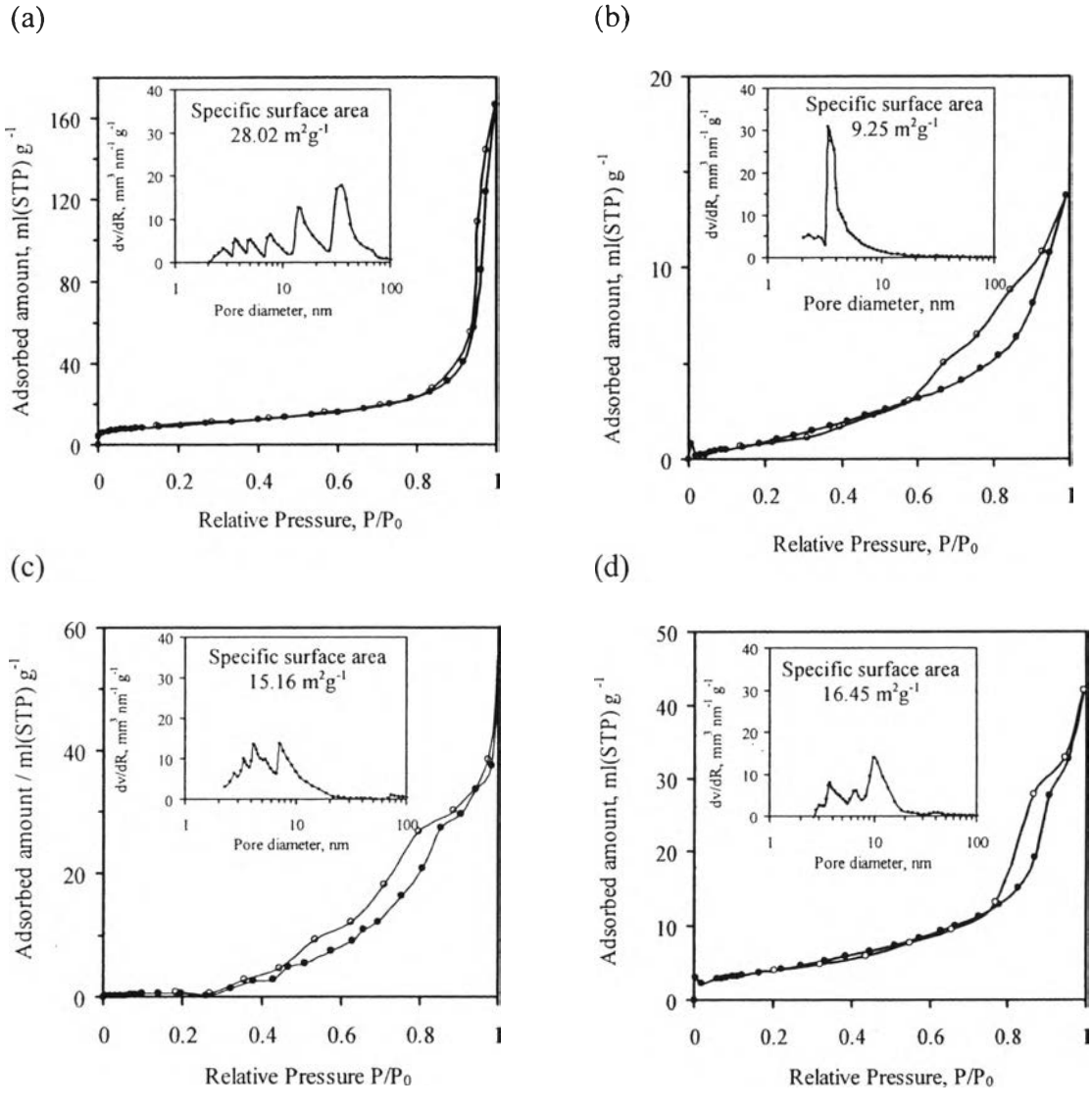

Figure 4.6 N_2 adsorption-desorption isotherms, specific surface area, and pore size distributions of (a) the commercial $SrTiO_3$ (Wako), and the synthesized $SrTiO_3$ (EtOH as a solvent, a calcination temperature of 700°C, a heating rate of 1°C min^{-1}, and a surfactant-to-TIPT molar ratio of 0.25:1) using different surfactants: (b) LAHC, (c) CTAB, and (d) CTAC.

The effects of solvent and surfactant on the specific surface areas and the pore size distributions of all synthesized $SrTiO_3$, as compared to the commercial $SrTiO_3$ determined by the N_2 adsorption-desorption isotherms, are shown in Figures 4.5 and 4.6, respectively. The isotherms of all synthesized $SrTiO_3$ showed a type IV IUPAC pattern with a hysteresis loop, indicating the existence of well-developed

mesopores in their assembled frameworks [28]. For the commercial $SrTiO_3$, its isotherm shows a type II IUPAC pattern without a hysteresis loop, indicating that its pore structure is a macropore (not a mesopore), as confirmed by a very broad and right-shift pore size distribution, as shown in Figure 4.5(a). Figures 4.5(b), 4.5(c), and 4.5(d) show the comparative results among the $SrTiO_3$ samples synthesized by using different solvents. It is clearly seen that the $SrTiO_3$ synthesized by using EtOH exhibited the narrowest pore size distribution, despite the lowest specific surface area, as compared to the other solvents (EG and the EtOH/EG mixture). The results can be explained in that the synthesis method using EtOH can give a faster solvent removal rate from the zero gel networks during the calcination step. The faster removal rate can cause a higher possibility of pore collapse. Another significant characteristic is that the $SrTiO_3$ synthesized by using EtOH exhibits the monomodal pore size distribution, while the $SrTiO_3$ synthesized by other studied solvents provided the multimodal pore size distribution, as shown in the insets of Figure 4.5. Because LAHC has a smaller molecular size than CTAB and CTAC, its micellar size is smaller than the others, resulting in a product that possesses smaller pore diameters, as well as the narrowest pore size distribution; but LAHC gives a lower specific surface area than those prepared by using CTAB and CTAC, as shown in Figure 4.6. In addition, as shown in the insets of Figure 4.6, only the LAHC surfactant provides the monomodal pore size distribution, indicating that LAHC is superior to the other investigated surfactants in contributing to more uniform pore structure.

The band gap energy, an important property of photocatalysts, can be determined through the plots between the Kubelka-Munk function $F(R)$ and λ, as described earlier. The plots between the Kubelka-Munk function $F(R)$ and λ of the $SrTiO_3$ photocatalysts prepared with different surfactants to be used to estimate their band gap energy (E_g) are shown in Figure 4.7. The results shows that the band gap wavelength (λ_g) of all synthesized $SrTiO_3$ are very close and shift to the higher wavelength (the red shift) when compared with the commercial $SrTiO_3$ band gap wavelength. Nevertheless, the $SrTiO_3$ synthesized by using LAHC tends to provide the lower E_g, as shown in Table 4.2. Interestingly, the E_g values of all synthesized $SrTiO_3$ samples are slightly lower than that of the commercial $SrTiO_3$ (Wako),

suggesting that the synthesized $SrTiO_3$ photocatalysts are theoretically more effective than the commercial one for light absorption.

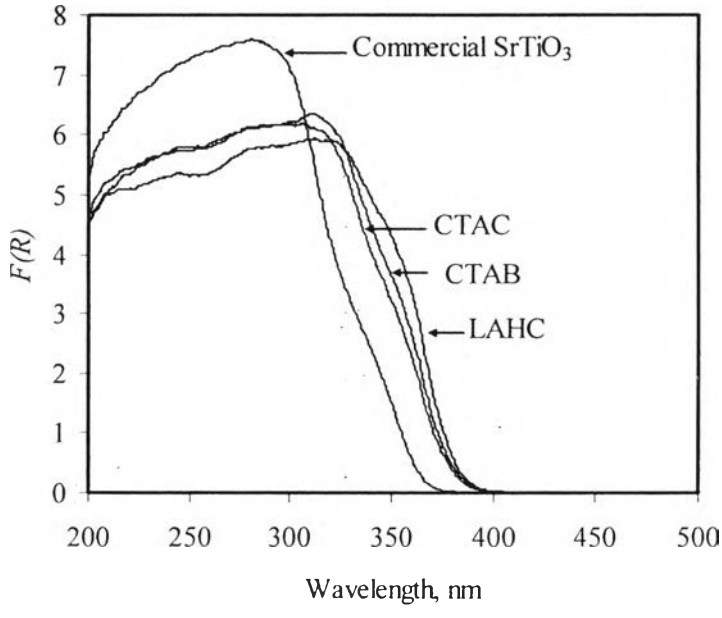

Figure 4.7 The plot between *F(R)* and λ of the $SrTiO_3$ samples (EtOH as a solvent, a calcination temperature of 700°C, a heating rate of 1°C min^{-1}, and a surfactant-to-TIPT molar ratio of 0.25:1) synthesized with different surfactants: LAHC, CTAB, and CTAC, as compared to the commercial $SrTiO_3$ (Wako).

Table 4.2 Band gap wavelength (λ_g), the band gap energy (E_g), and crystallite size of $SrTiO_3$ synthesized by using different surfactants: LAHC, CTAB, and CTAC, as compared to commercial $SrTiO_3$ (Wako)

Photocatalyst	Surfactant type	λ_g (nm)	E_g (eV)	Crystallite size (nm)
Synthesized $SrTiO_3$	LAHC	386	3.21	35
	CTAB	382	3.25	32
	CTAC	380	3.26	28
Commercial $SrTiO_3$	-	360	3.44	33

According to the results mentioned above, the synthesized mesoporous-assembled $SrTiO_3$ nanocrystals prepared by using EtOH as a solvent and LAHC as a structure-directing surfactant possessed the most homogeneous pore size and the highest purity, and tended to provide the lowest band gap energy. Hence, LAHC was selected for further investigation of the effect of the LAHC-to-TIPT molar ratio. The effects of the LAHC-to-TIPT molar ratio on the pore size distribution and specific surface area are shown in Figure 4.8. When the LAHC-to-TIPT molar ratio increased, the pore size distribution and the averaged diameter tended to increase, whereas the specific surface area decreased. The results can be explained in that an increase in the LAHC-to-TIPT molar ratio (higher surfactant concentration) leads to an increase in both the size and number of surfactant micelles, and consequently tends to increase the pore collapse during the calcination step, resulting in a product that possessed a lower specific surface area, and broader and more multimodal pore size distribution. It was experimentally found that the $SrTiO_3$ photocatalyst prepared at a LAHC-to-TIPT molar ratio of 0.25:1 provided the monomodal and narrowest pore size distribution, as well as the highest specific surface area. The plots between $F(R)$ and λ of the synthesized $SrTiO_3$ samples prepared by using different LAHC-to-TIPT molar ratios, as compared to the commercial $SrTiO_3$, are shown in Figure 4.9. As shown in Table 4.3, each synthesized $SrTiO_3$ photocatalyst has the same λ_g and the same estimated value of E_g, indicating that the LAHC-to-TIPT molar ratio did not affect the band gap energy of the synthesized $SrTiO_3$ photocatalysts.

(a)

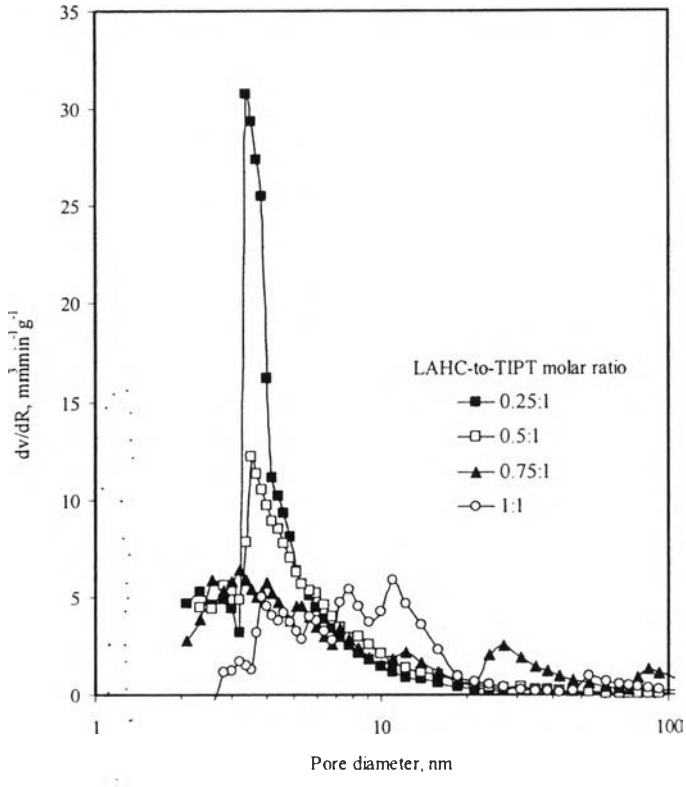

(b)

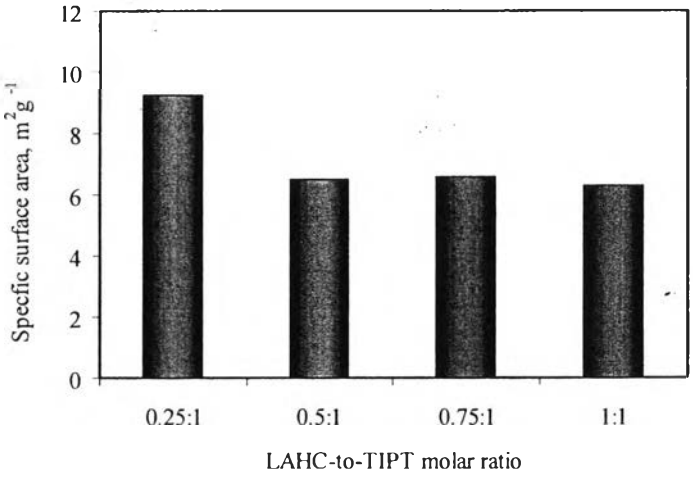

Figure 4.8 (a) Pore size distribution and (b) specific surface area of the $SrTiO_3$ samples prepared with different LAHC-to-TIPT molar ratios using EtOH as a solvent, 700°C calcination temperature, and 1°C min^{-1} heating rate.

Table 4.3 Band gap wavelength (λ_g), the band gap energy (E_g), and crystallite size of $SrTiO_3$ synthesized by using different LAHC-to-TIPT molar ratios: 0.25:1, 0.5:1, 0.75:1, and 1:1, as compared to commercial $SrTiO_3$ (Wako)

Photocatalyst	LAHC-to-TIPT molar ratio	λ_g (nm)	E_g (eV)	Crystallite size (nm)
Synthesized $SrTiO_3$	0.25:1	386	3.21	35
	0.5:1	386	3.21	35
	0.75:1	386	3.21	35
	1:1	386	3.21	35
Commercial $SrTiO_3$	-	360	3.44	33

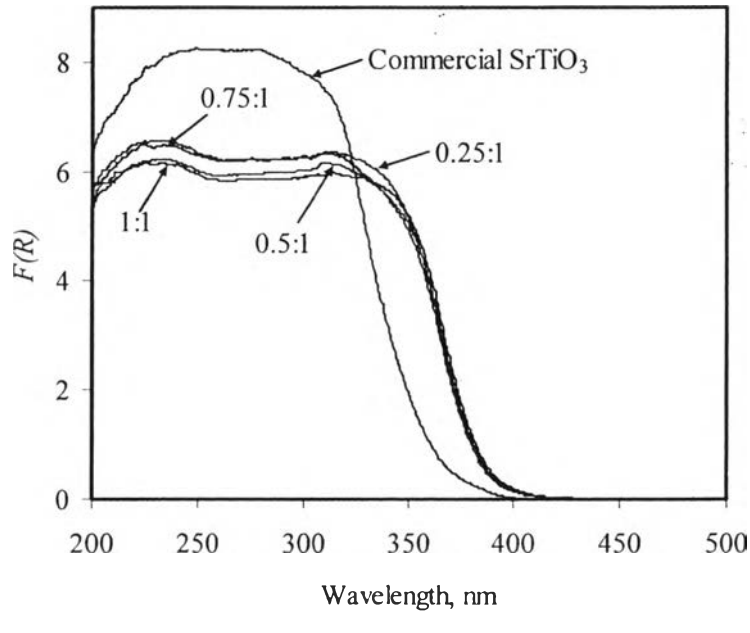

Figure 4.9 Plot between $F(R)$ and λ of the $SrTiO_3$ samples (EtOH as a solvent, a calcination temperature of 700°C, and a heating rate of 1°C min^{-1}) prepared with different LAHC-to-TIPT molar ratios, as compared to commercial $SrTiO_3$ (Wako).

The morphologies of the $SrTiO_3$ photocatalyst synthesized under the optimum conditions (EtOH as a solvent, LAHC as a structure-directing surfactant, a heating rate of 1°C min^{-1}, and a LAHC-to-TIPT molar ratio of 0.25:1) at different calcination temperatures and the commercial $SrTiO_3$ were observed by a transmission electron microscope (TEM). As shown in Figure 4.10, the TEM images show that the commercial $SrTiO_3$ had non-uniform particle sizes ranging from 20 to 200 nm (Figure 4.10(a)), while the synthesized $SrTiO_3$ photocatalysts seemed to have much more uniform particle sizes with smaller size in the range of 20-40 nm (Figure 4.10(b)-(d)). For the calcination temperature range from 600 to 700°C, the TEM results showed that the increase in the calcination temperature resulted in the slight decrease in the particle size. The estimated particle size of the synthesized $SrTiO_3$ obtained from the TEM analysis, which is approximately 20-40 nm, is in good agreement with the crystallite size calculated from the XRD pattern, as exemplified in Tables 4.2 and 4.3 for the synthesized $SrTiO_3$ calcined at 700°C, indicating that the single crystal was formed by using the synthesis method described in this study. According to the N_2 adsorption-desorption and TEM results, it is worth noting that the mesoporous structure of the synthesized $SrTiO_3$ can be attributed to the pores formed between the nanocrystalline $SrTiO_3$ particles due to their assembly, which is in the same track as the widely investigated mesoporous TiO_2 reported in literature [8-10, 29-34].

In addition, when considering the quantization effect, the band gap energy of the semiconductor photocatalyst depends on its particle size as the band gap of the photocatalyst increases with decreasing the particle size. The estimated E_g of the synthesized $SrTiO_3$ photocatalysts showed the opposite trend to effect in the quantization effect when compared with the estimated E_g of the commercial $SrTiO_3$ (Wako). As shown in Figure 4.10 and Tables 4.2 and 4.3, the synthesized $SrTiO_3$ photocatalysts have smaller particle sizes (with grain of each particle as single crystal, as above explained) than the commercial $SrTiO_3$ (Wako), but their E_g values are lower than that of the commercial $SrTiO_3$. This unexpected characteristic may be explained in that the decrease in E_g is probably due to the tight aggregation of the

single crystals into larger assembly so as to behave like a large crystal, resulting in the ability to absorb light with longer wavelengths.

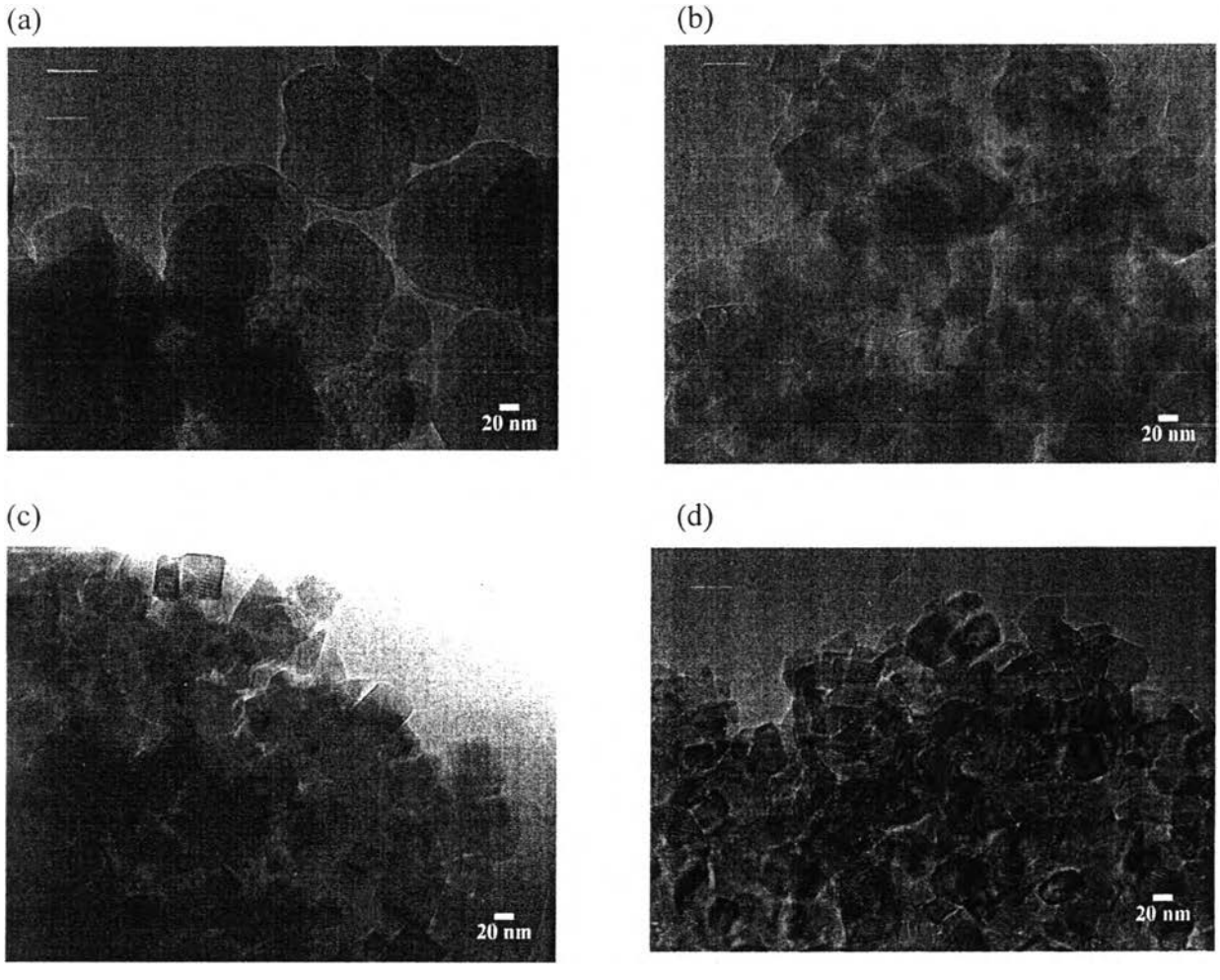

Figure 4.10 TEM images of (a) the commercial $SrTiO_3$ (Wako), and the synthesized $SrTiO_3$ (EtOH as a solvent, a heating rate of 1°C min^{-1}, and a LAHC-to-TIPT molar ratio of 0.25:1) calcined at different calcination temperatures: (b) 600°C, (c) 650°C, and (d) 700°C.

4.3.3 Photocatalytic Activity Results

The photocatalytic activity of the mesoporous-assembled $SrTiO_3$ nanocrystal photocatalysts synthesized by using EtOH as a solvent, LAHC as a structure-directing surfactant, a heating rate of 1°C min^{-1}, and a TIPT-to-LAHC

molar ratio of 1:0.25, and of the commercial $SrTiO_3$ (Wako), for the decomposition of methyl orange, are determined from the maximum absorption wavelength of 464 nm of methyl orange solution. The effect of calcination temperature on the photocatalytic activity of the synthesized mesoporous-assembled $SrTiO_3$ nanocrystals as compared to the commercial $SrTiO_3$ (Wako) is shown in Figure 4.11. As the calcination temperature increased from 600 to 700°C, the percentage of methyl orange degradation and the pseudo-first-order rate constant increased substantially and reached a maximum value at 700°C. However, when the calcination temperature exceeded 700°C, both of the process parameters decreased abruptly. As shown in Figure 4.11(a), the calcination temperature strongly affects the photocatalytic activity, and the mesoporous-assembled $SrTiO_3$ synthesized at this optimum temperature of 700°C provides the complete degradation of methyl orange at a reaction time of 3 h. This can be explained in that both the specific surface area and the crystallinity are clearly governed by the calcination temperature, as seen in Figures 4.4 and 4.11(b). The effect of calcination temperature can be divided into three regions. Firstly, for the calcination temperature range from 600 to 650°C, the increase in the temperature led to increases in both the crystallinity and the specific surface area, which resulted in an increase in the photocatalytic activity. Secondly, for the calcination temperature range from 650 to 700°C, the increase in the temperature led significantly to an increase in the crystallinity but to a decrease in the specific surface area. In this temperature range, the increase in the photocatalytic activity due to the positive effect of the increasing crystallinity might exceed the negative effect of the decrease in specific surface area, as indicated by both the increase in the percentage of methyl orange degradation and the reaction rate constant. Thirdly, for the calcination temperature range from 700 to 750°C, the increase in the temperature led to a slight increase in the crystallinity but to a significant decrease in the specific surface area. The decrease in the overall photocatalytic activity in this temperature range results from the drastic reduction of the specific surface area. The results suggest that the photocatalytic activity of the $SrTiO_3$ photocatalyst depends on both specific surface area and crystallinity.

(a)

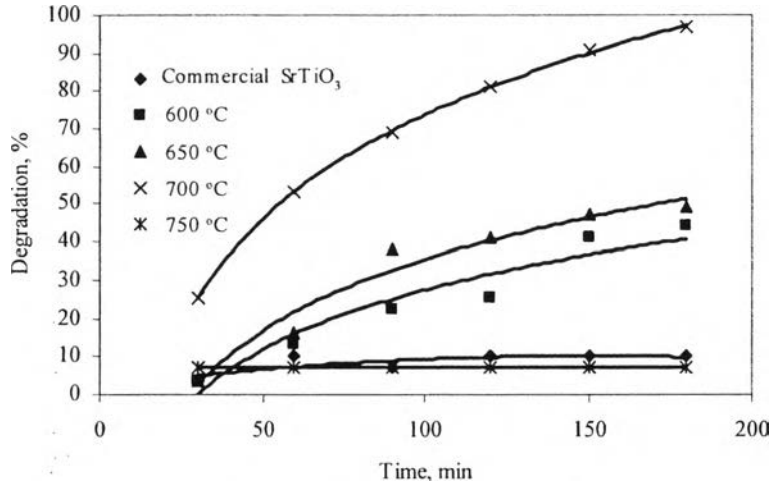

(b)

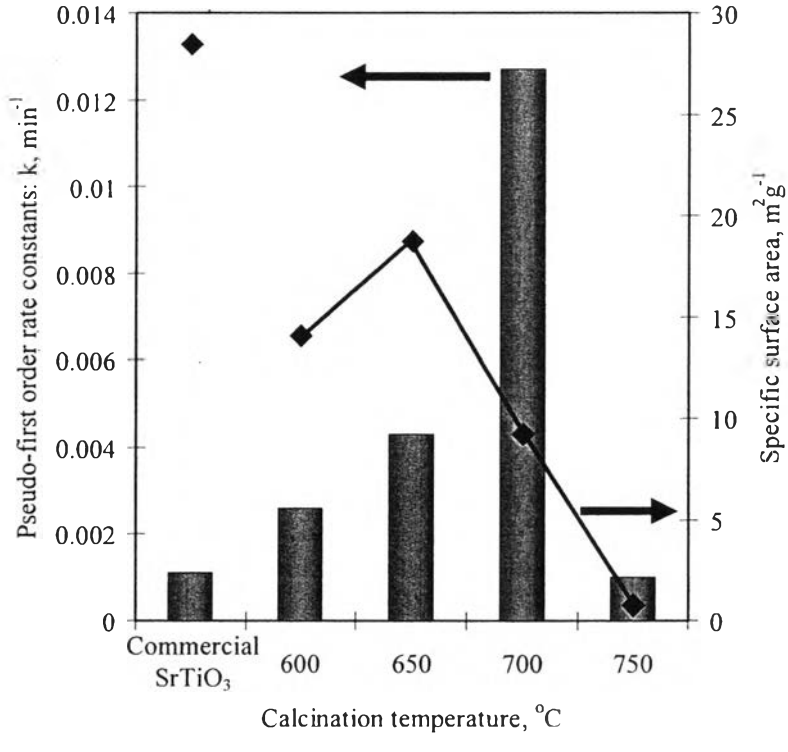

Figure 4.11 (a) Time course of the percentage of methyl orange degradation over the synthesized $SrTiO_3$ photocatalysts and (b) the specific surface area and the pseudo-first-rate constant of the synthesized $SrTiO_3$ photocatalysts, as compared to the commercial $SrTiO_3$ (Wako). The synthesized $SrTiO_3$ photocatalysts were prepared under the optimum conditions (EtOH as a solvent, a heating rate of 1°C min^{-1}, and a LAHC-to-TIPT molar ratio of 0.25:1) at different calcination temperatures.

Thus, the synthesis conditions, especially the calcination temperature, should be optimized to achieve a good balance between the specific surface area and the crystallinity of the photocatalysts. In comparisons of the photocatalytic activity of the commercial $SrTiO_3$ and the synthesized mesoporous-assembled $SrTiO_3$ nanocrystals as shown in Figure 4.11, even though the commercial $SrTiO_3$ possesses high crystallinity (see Figure 4.2) with a high specific surface area (see Figure 4.11(b)), its predominant macroporous structure (see Figure 4.5(a)), non-uniform particle sizes (see Figure 4.10(a)), and broad pore size distribution (see Figure 4.5(a)) could contribute to a very poor photocatalytic activity, which was about 13 times lower than that of the synthesized $SrTiO_3$ calcined at 700°C. The very low photocatalytic activity of the commercial $SrTiO_3$ might be also due to its large particle size proportion, since the larger particle has less ability to absorb light when compared with the smaller one, leading to the decrease in the overall light absorption, and also tends to provide higher bulk electron-hole recombination possibility, resulting in less amount of effective species for subsequent photocatalytic reactions [35]. The results suggest that the particle size and its uniformity are very indispensable, affecting the photocatalytic activity of the $SrTiO_3$ photocatalysts.

The effect of the LAHC-to-TIPT molar ratio on the photocatalytic activity of the synthesized $SrTiO_3$ photocatalyst is shown in Figure 4.12. The $SrTiO_3$ synthesized by using a LAHC-to-TIPT molar ratio of 0.25:1 exhibited the highest specific surface area, resulting in the highest percentage of methyl orange degradation, as well as the highest pseudo-first-order rate constant. The results confirm that the photocatalytic activity depends on both the specific surface area and mesoporous uniformity, since the LAHC-to-TIPT molar ratio of 0.25:1 provided the most uniform and monomodal pore size distribution of the synthesized $SrTiO_3$, as clearly seen in Figure 4.8.

Finally, it is worth deducing that the mesoporous-assembled $SrTiO_3$ nanocrystals synthesized at a calcination temperature of 700°C, a heating rate of 1°C min^{-1}, a LAHC-to-TIPT molar ratio of 0.25:1, and using EtOH as a solvent, which possessed the most homogenous pore dimensions, the highest purity, and the optimum balance between the crystallinity and the specific surface area, showed the highest photocatalytic activity in the degradation of methyl orange.

(a)

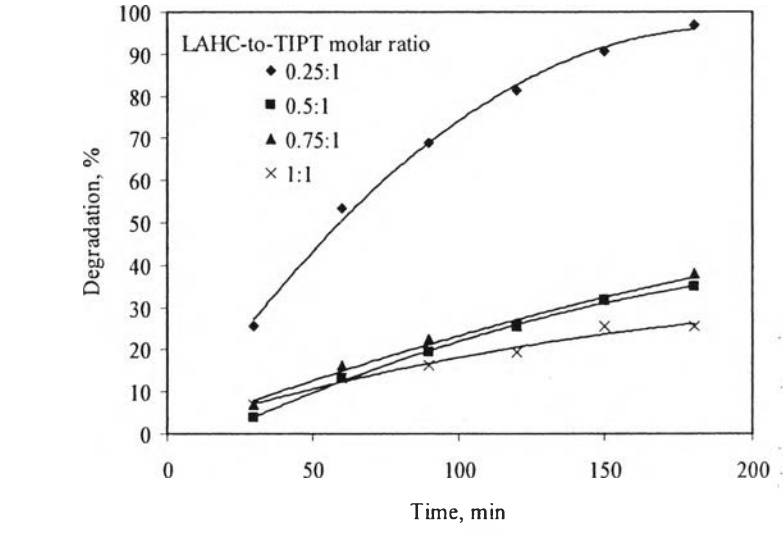

(b)

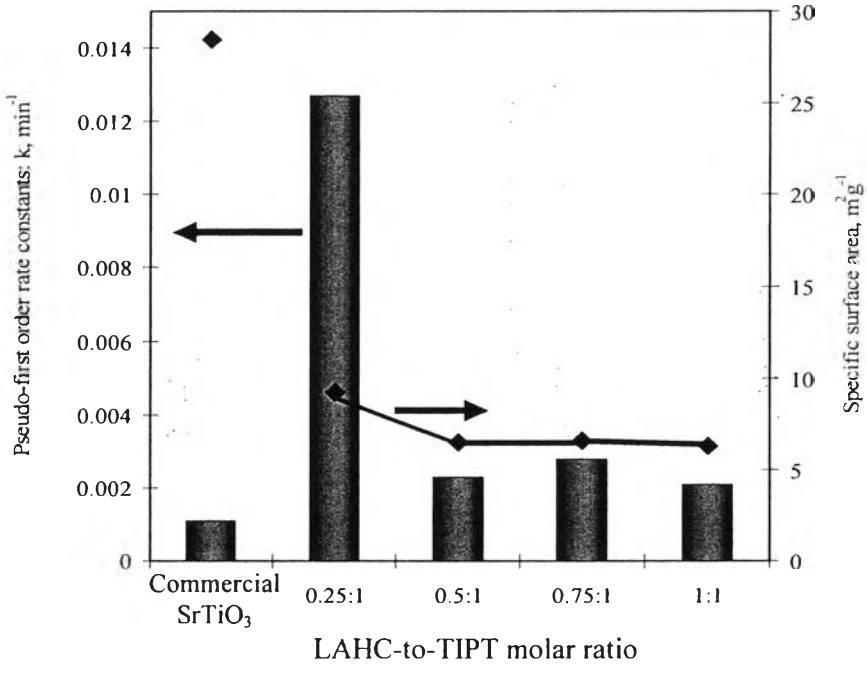

Figure 4.12 (a) Time course of the percentage of methyl orange degradation over the synthesized $SrTiO_3$ photocatalysts and (b) the specific surface area and the pseudo-first-rate constant of the synthesized $SrTiO_3$ photocatalysts, as compared to the commercial $SrTiO_3$ (Wako). The synthesized $SrTiO_3$ photocatalysts were prepared under the optimum conditions (EtOH as a solvent, a calcination temperature of 700°C, and a heating rate of 1°C min^{-1}) at different LAHC-to-TIPT molar ratios.

4.4 Conclusions

The mesoporous-assembled $SrTiO_3$ nanocrystal photocatalyst was successfully synthesized via the sol-gel method with the aid of structure-directing surfactant. The different solvents resulted in different gel formation characteristics and different amounts of water required for the gel formation. The use of EtOH as the solvent yielded a $SrTiO_3$ photocatalyst with a higher purity than that synthesized using EG or the EtOH/EG mixture. The N_2 adsorption-desorption isotherms of the synthesized $SrTiO_3$ photocatalysts showed a single and well-defined step and a clear hysteresis loop in the desorption branch, indicating the mesoporous characteristic. The pore size distribution was found to be very narrow and monomodal when LAHC was used as a structure-directing surfactant. The pore size distribution and surface area of the synthesized $SrTiO_3$ photocatalysts can be controlled by the adjustment of the LAHC-to-TIPT molar ratio. From the methyl orange photodegradation results, the photocatalytic activity of the mesoporous-assembled $SrTiO_3$ nanocrystals calcined at 700°C reached a maximum. The photocatalytic activity was also found to depend on the LAHC-to-TIPT molar ratio, exhibiting the highest photocatalytic activity at a ratio of 0.25:1. From the results, the photocatalytic activity of the $SrTiO_3$ photocatalyst depended on specific surface area, crystallinity, and pore characteristics. The mesoporous-assembled structure with a pore uniformity of $SrTiO_3$ photocatalyst plays an important role affecting the photocatalytic activity.

4.5 Acknowledgments

This work was supported by a Project on Faculty Development in Shortage Area Scholarship (Thailand), the National Excellence Center for Petroleum, Petrochemicals, and Advanced Materials (Thailand), the Research Unit of Applied Surfactants for Separation and Pollution Control, Chulalongkorn University (Thailand), and Institute of Advanced Energy, Kyoto University (Japan).

4.6 References

[1] L. Hinda, P. Eric, H. Ammar., K. Mohamed, E. Elimame., G. Cantal, H. Jean-Marie, Appl. Catal. B: Environ. 39 (2002) 75.

[2] I. K. Konstantinou, T. A. Albanis, Appl. Catal. B: Environ. 49 (2004) 1.

[3] S. Ahuja, T.R.N. Kutty, J. Photochem. Photobiol. A: Chem. 97 (1996) 99.

[4] S. Vaidyanathan, K.R. Ryan, E.W. Eduardo, Ind. Eng. Chem. Res. 45 (2006) 2187.

[5] D.L. Liao, B.Q. Liao, J. Photochem. Photobiol. A: Chem. 187 (2007) 363.

[6] T. Ohno, T. Tsubota, Y. Nakamura, K. Sayama, Appl. Catal. A: Gen. 288 (2005) 74.

[7] J. Poth, R. Haberkorn, H.P. Beck, J. European Ceram. Soc. 20 (2000) 715.

[8] T. Sreethawong, Y. Suzuki, S. Yoshikawa, Catal. Commun. 6 (2005) 119.

[9] S. Sakulkhaemaruethai, Y. Suzuki, S. Yoshikawa, J. Ceram. Soc. Jpn. 112 (2004) 547.

[10] T. Sreethawong, Y. Suzuki, S. Yoshikawa, J. Solid State Chem. 178 (2005) 329.

[11] M. E.Ebrahimi, M. Allahverdi, A. Safari, J. Am. Ceram. Soc. 88 (2005) 2129.

[12] K. Masato, O. Toru, A. Momoko, J. Sol-Gel Sci. Technol. 12 (1998) 95.

[13] S. Zhang, J. Liu, Y. Han, B. Chen, X. Li, Mater. Sci. Eng. B: Solid State Mater. Adv. Technol. 110 (2004) 11.

[14] J. Wang, S. Yin, T. Sato, J. Photochem. Photobiol. A: Chem. 187 (2007) 72.

[15] H. Cui, M. Zayat, D. Levy, J. Non-Cryst. Solids 353 (2007) 1011.

[16] D. A. Ward, E. I. Ko, Ind. Eng. Chem. Res. 34 (1996) 421.

[17] L.A. García-Cerda, O.S. Rodríguez-Fernández, P.J. Reséndiz-Hernández, J. Alloy. Compd. 369 (2004) 182.

[18] M.P. Pileni, Nature Mater. 2 (2003) 145.

[19] L. Motte, M.P. Pileni, Appl. Surf. Sci. 164 (2000) 60.

[20] M. Moumen, I. Lisiecki, M.P. Pileni, Supramol. Sci. 2 (1995) 161.

[21] D.L. Liao, B.Q. Liao, Inter. J. Chem. React. Eng. 5:A24 (2007).

[22] T. Sreethawong, Y. Yamada, T. Kobayashi, S. Yoshikawa, J. Mol. Catal. A: Chem. 241 (2005) 23.

[23] K. Cassiers, T. Linssen, K. Aerts, P. Cool, O. Lebedev, G. V. Tendeloo, R. V. Griekenb, E. F. Vansanta, J. Mater. Chem. 13 (2003) 3033.

[24] M. M. Yusuf, H. Imai, H. Hirashima, J. Sol-Gel Sci. Technol. 28 (2003) 97.

[25] T. Puangpetch, T. Sreethawong, S. Chavadej, S. Yoshikawa, Mesoporous $SrTiO_3$ Photocatalyst Synthesized via Surfactant-Assisted Templating Sol-Gel Method and Its Methyl Orange Photodegradation Activity, The 4th Asia Pacific Congress on Catalysis (APCAT 4), 6-8 December 2006, Singapore.

[26] C. J. Brinker, G.W. Scherer, Sol-Gel Science, Academic Press, New York, 1989.

[27] J. V. Smith (Ed.), X-Ray Powder Data File, American Society for Testing Materials, Philadelphia, PA, 1960.

[28] F. Rouquerol, J. Rouquerol, K. Sing, Adsorption by Powders and Porous Solids: Principles, Methodology and Applications, Academic Press, San Diego, 1999.

[29] J. C. Yu, J. Yu, W. Ho, L. Zhang, Chem. Commun. 19 (2001) 1942.

[30] Y. Zhang, A. Weidenkaff, A. Reller, Mater. Lett. 54 (2002) 375.

[31] J. Yu, J. C. Yu, M. K. P. Lueng, W. Ho, B. Cheng, X. Zhao, J. Zhao, J. Catal. 217 (2003) 69.

[32] Y. Zhang, H. Zhang, Y. Hu, Y. Wang, J. Solid State Chem. 177 (2004) 3490.

[33] Y. V. Kolen'ko, V. D. Maximov, A. V. Garshev, P. E. Meskin, N. N. Oleynikov, B. R. Churagulov, Chem. Phys. Lett. 388 (2004) 411.

[34] Q. Sheng, Y. Cong, S. Yuan, J. Zhang, M. Anpo, Micropor. Mesopor. Mater. 95 (2006) 220.

[35] H. Lin, C. P. Huang, W. Li, C. Ni, S. I. Shah, Y. H. Tseng, Appl. Catal. B: Environ. 68 (2006) 1.